Development of novel biosensors to study receptor-mediated activation of the G-protein α subunits G_s and G_{olf}

Received for publication, June 7, 2017, and in revised form, October 2, 2017 Published, Papers in Press, October 17, 2017, DOI 10.1074/jbc.M117.800698

Hideaki Yano[‡1], **Davide Provasi**[§], **Ning Sheng Cai**[‡], **Marta Filizola**[§], **Sergi Ferré**[‡], **and Jonathan A. Javitch**[¶‖2]

From the [‡]*National Institute on Drug Abuse, Baltimore, Maryland 21224, the* [§]*Department of Pharmacological Sciences, Icahn School of Medicine at Mount Sinai, New York, New York 10029, the* [¶]*Departments of Psychiatry and Pharmacology, College of Physicians & Surgeons, Columbia University, New York, New York 10032, and the* [‖]*Division of Molecular Therapeutics, New York State Psychiatric Institute, New York, New York 10032*

Edited by Henrik G. Dohlman

$G\alpha_s$ (G_s) and $G\alpha_{olf}$ (G_{olf}) are highly homologous G-protein α subunits that activate adenylate cyclase, thereby serving as crucial mediators of intracellular signaling. Because of their dramatically different brain expression patterns, we studied similarities and differences between their activation processes with the aim of comparing their receptor coupling mechanisms. We engineered novel luciferase- and Venus-fused $G\alpha$ constructs that can be used in bioluminescence resonance energy transfer assays. In conjunction with molecular simulations, these novel biosensors were used to determine receptor activation–induced changes in conformation. Relative movements in G_s were consistent with the crystal structure of β_2 adrenergic receptor in complex with G_s. Conformational changes in G_{olf} activation are shown to be similar to those in G_s. Overall the current study reveals general similarities between G_s and G_{olf} activation at the molecular level and provides a novel set of tools to search for G_s- and G_{olf}-specific receptor pharmacology. In view of the wide functional and pharmacological roles of G_s- and G_{olf}-coupled dopamine D_1 receptor and adenosine A_{2A} receptor in the brain and other organs, elucidating their differential structure–function relationships with G_s and G_{olf} might provide new approaches for the treatment of a variety of neuropsychiatric disorders. In particular, these novel biosensors can be used to reveal potentially therapeutic dopamine D_1 receptor and adenosine A_{2A} receptor ligands with functionally selective properties between G_s and G_{olf} signaling.

The G_s family of $G\alpha$ proteins, comprised of two highly homologous G_s and G_{olf} subtypes, positively couple to adenylate cyclase (thus, "s" for stimulatory). Upon activation, both G_s and G_{olf} promote cAMP production and subsequent signaling events such as activation of the PKA cascade. G_s is ubiquitously expressed in most organs, whereas G_{olf} is mainly restricted to the brain. Moreover, within the brain, G_s and G_{olf} exhibit distinct expression patterns. G_s is uniformly expressed throughout the brain, except in the striatum where its expression is very low. In contrast, G_{olf} is highly expressed in the striatum and olfactory tubercle, as well as in the hippocampus and cerebellum to a lesser extent (41). The contrast in tissue expression for G_s and G_{olf} is quite dramatic and unique among other $G\alpha$ homologs (*e.g.* G_i *versus* G_o, G_q *versus* G_{11}, and G_{12} *versus* G_{13}) (1), making G_s and G_{olf} fascinating molecular targets with regard to their corresponding functions, particularly in terms of D_1 receptor (D1R)-mediated[3] and A_{2A} receptor (A2AR)-mediated signaling in the striatum compared with other brain regions.

Conformational changes associated with GPCR activation have been revealed in remarkable detail by the crystal structure of agonist-bound β_2 adrenergic receptor (β2AR) in complex with G_s, by complementary spectroscopy studies, as well as by related molecular dynamics studies (2–5). However, the extent to which conformational changes in G protein are conserved in living cells, as well as across different receptors and different G-protein isoforms, remains unclear. In particular, little is known about the G_s homolog G_{olf} in terms of its functional similarities and differences. Despite their different expression patterns, the high degree of homology in amino acid sequences (89% identity) has led to the assumption that G_s and G_{olf} function essentially identically at both the molecular and cellular levels. For this reason, as well as the fact that G_{olf} expression is typically poor in heterologous cells, G_s functional assays have been used as surrogates for G_{olf} activation, begging the question of just how similar these processes are. The answer may provide specific ways to target selectively physiological functions mediated by either G_s or G_{olf} signaling.

In the current study, we first focused on β2AR-G_s activation in intact cells to investigate conformational changes of different domains of G_s. Using bioluminescence resonance energy transfer (BRET)-based assays, we assessed movements both within the G protein, as well as between the receptor and $G\alpha$ subunit.

This work was supported by Intramural funds of the National Institute on Drug Abuse (to S. F.), a fellowship from the Japan Society for the Promotion of Science (to H. Y.), and National Institutes of Health Grants DA022413 and MH54137 (to J. A. J.) and DA026434 (to M. F.). The authors declare that they have no conflicts of interest with the contents of this article. The content is solely the responsibility of the authors and does not necessarily represent the official views of the National Institutes of Health.

This article contains supplemental Tables S1–S3 and Figs. S1–S7.

[1] To whom correspondence may be addressed. Tel.: 443-740-2612l; E-mail: yanoh@nih.gov.

[2] To whom correspondence may be addressed. Tel.: 646-774-8600; E-mail: jaj2@columbia.edu.

[3] The abbreviations used are: D1R, dopamine D_1 receptor; D2R, dopamine D_2 receptor; BRET, bioluminescence resonance energy transfer; A2AR, adenosine A_{2A} receptor; β1AR, β_1 adrenergic receptor; β_2AR, β_2 adrenergic receptor; PDB, Protein Data Bank; M1R, muscarinic M1 receptor; Rluc8, *Renilla* luciferase 8; RET, resonance energy transfer; RMSD, root mean square deviation.

Using a library of novel G_s biosensors with either luciferase or GFP variants inserted at various positions throughout the structure, we studied conformational changes in living cells and compared the results to the crystal structures of the closed and open conformations of G_s (2, 6). We then studied conformational changes in G_s induced by activation of the D1R, A2AR, and β_1 adrenergic receptor (β1AR). Next, taking advantage of the significant homology, we created a series of G_{olf} biosensor constructs with insertions at the same nine positions used for G_s. Agonist-induced conformational changes in G_{olf} were compared with those in G_s. Finally, G_{olf} assay optimization was carried out for D1R. Our analysis using these G_s biosensors suggests that conformational changes within the G_s heterotrimer are similar when induced by different G_s-coupled receptors. Comparison between the G_s and G_{olf} sensor readouts also indicates a very similar regulation of activation by endogenous agonists. Using this set of G_s and G_{olf} biosensors, the efficacy and potency of agonists, as well as the activation preference between G_s and G_{olf}, can be studied in relation to structural changes and subsequent effector activation. Our results with D1R establish that these biosensors represent a novel pharmacological tool to study structure-function relationships comparing G_s and G_{olf}.

Results

Sensor insertion positions to assess the open and closed conformations of G_s

A dramatic structural change is apparent between the closed (PDB code 1AZT) and open (PDB code 3SN6) states of the G_s heterotrimer, particularly in the α-helical domain (Fig. 1*A*). To detect such conformational changes upon G-protein activation, biosensors were constructed in which Rluc or mVenus were inserted at nine different insertion positions in the loop motifs of different domains in G_s (Fig. 1, *A* and *B*). The insertion positions (*i.e.* loop regions) were selected to avoid structural perturbations. Position 7 is located between the N terminus and αN. Positions 67 and 71 are situated in the linker-loop motif, which was not resolved in the crystal structures; they are in the hinge domain that connects the Ras-like catalytic domain and α-helical domain. Insertion of GFP at position 71 of G_s has been functionally validated previously (7). Positions 99, 154, and 175 are located in the α-helical domain (position 99, proximal; positions 154 and 175, distal), whereas positions 305, 338, and 349 are located in the Ras-like domain, avoiding the catalytic core. Insertion of mVenus (YFP variant) or Rluc8 at these positions led to similar levels of expression based on levels of fluorescence for the mVenus constructs and luminescence for the RLuc8 constructs (data not shown).

G_s biosensors detect distinct conformational changes upon activation

Relative movements between G_s and $G_{\gamma 2}$ upon receptor activation were studied, similarly to previous analysis of G_i activation using G_i biosensors with insertions at positions 60, 91, and 122 (aligned with positions 67, 99, and 131 in G_s, respectively) (8, 9). Of the nine insertion constructs we created, when co-expressed with β2AR (Fig. 2*A*), G_s with insertions at positions 305, 338, and 349 failed to show significant isoproterenol-induced BRET changes, although the fluorescence and luminescence levels were not significantly different from other biosensors. Insertion positions, 67, 71, 99, and 154, on the other hand, produced substantial agonist-induced BRET changes. When co-expressed with β2AR (Fig. 2*A*), isoproterenol increased BRET between Gs67-Rluc and γ2-GFP10 or Gs71-Rluc and γ2-GFP10, consistent with greater proximity of the sensors in the two subunits. In contrast, Gs99-Rluc and γ2-GFP10 or Gs154-Rluc and γ2-GFP10 decreased BRET, indicating an increase in distance. When the donor–acceptor pair was reversed, the directions of BRET change in G_s-Venus-γ2-Rluc remained the same (supplemental Fig. S1). Furthermore, when co-expressed with D1R (Fig. 2*B*), the directions of change for all the positions were consistent with the β2AR results. Activation of adrenergic β1AR and adenosine A2AR also showed the same directionality as D1R and β2AR (supplemental Fig. S2).

Although the β1 and γ2 subunits are widely expressed in the brain, β2 and γ7 subunits have been reported to be enriched in the striatum where they play an important role in D1R- and A2AR-mediated signaling (10–13). Therefore, β1/γ2-Venus or β1/γ2-GFP10 was replaced with β2/γ7-Venus or β2/γ7-GFP10 to study D1R activation. The directionalities of BRET change were the same for the β1/γ2 and β2/γ7 pairs (supplemental Fig. S1). When tested for β2AR with β1/γ2 or β2/γ7, the same directionalities were also observed (supplemental Fig. S1).

Venus-fused G_s constructs were also tested for their use in measuring receptor–Gα engagement (supplemental Fig. S3). With both β2AR and D1R, sensor position 154 showed the largest dynamic range for agonist-induced effects, ~3-fold greater than that observed for the previously studied position 71 insertion (7–9) (supplemental Fig. S3).

Simulated conformational trajectories reveal a movement in the hinge loop

To provide a structural context to our BRET results, we used the closed crystal structure of G_s (6) and the open conformation of the G_s crystal structure in complex with β2AR (2) as beginning and ending structures, respectively, to simulate domain movement between the closed and open crystal structures of G_s (Fig. 2, *C* and *D*). A missing loop (residues 66–72) of the closed G_s crystal structure was built using the Rosetta loop prediction algorithm. The best scoring conformation was extracted and equilibrated in the context of the protein by a 20-ns all-atom MD simulation. Adiabatic biased MD was then employed to generate a continuous, low-energy transition path starting from the closed G_s crystal structure and reducing the root mean square deviation from the open G_s crystallographic conformation. Distances between the Cα atoms of experimental insertion points for the different configurations are reported in supplemental Table S1, showing the general agreement with changes in BRET values. The hinge loop (positions 67 and 71), buried partially between Ras-like and α-helical domains in closed state, opens and moves closer to the γ subunit in the open state. In contrast, the α-helical domain (positions 99 and 154) moves away from the γ subunit.

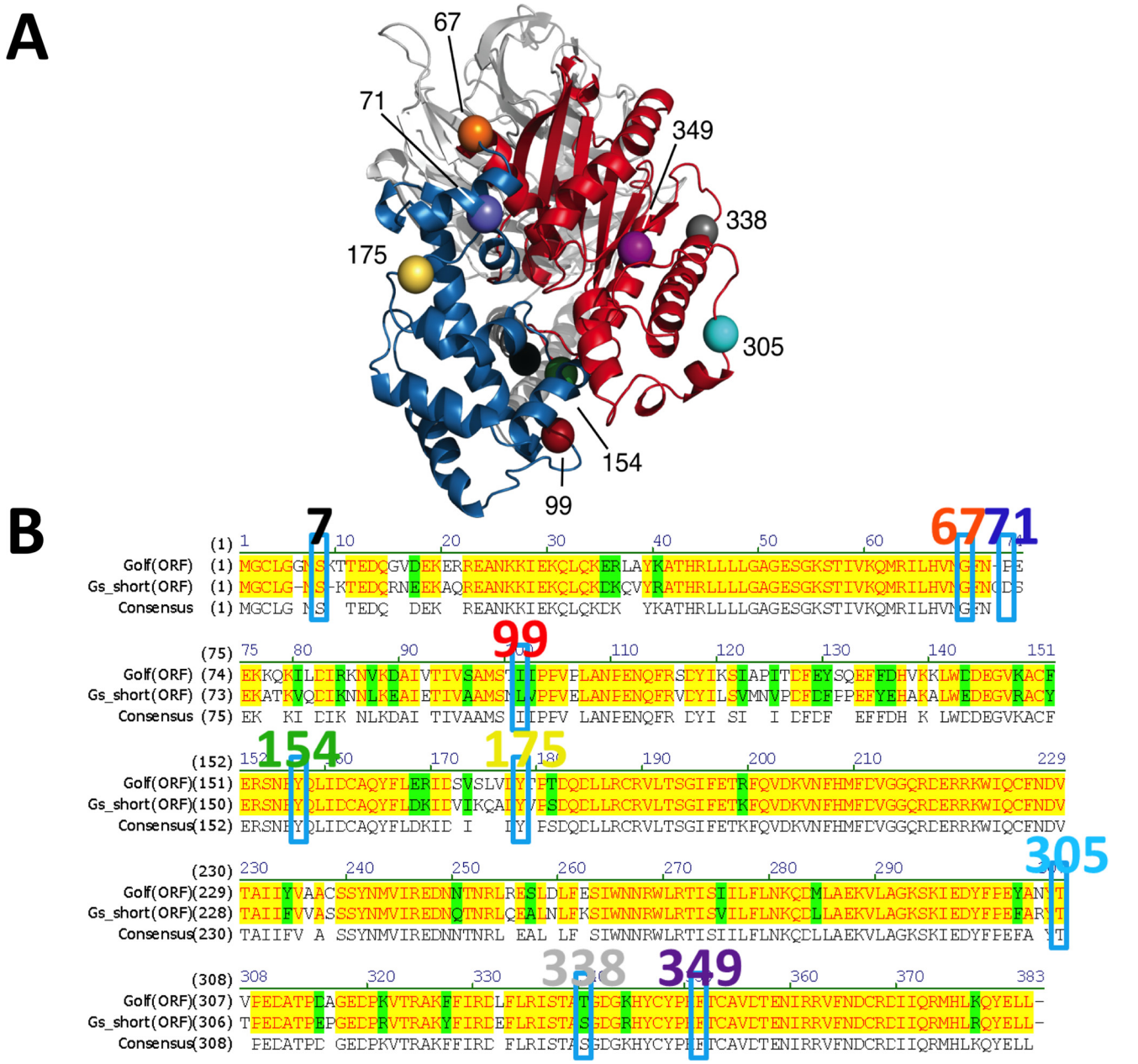

Figure 1. *A*, location of the insertion points of six selected probe positions resolved in the inactive/closed (PDB code 1AZT) crystal structure of G_s are shown at positions 99 (*red*), 154 (*green*), 175 (*yellow*), 305 (*light blue*), 338 (*gray*), and 349 (*purple*). The α-helical and Ras-like domains of Gα are in *blue* and *red*, respectively, whereas Gβ and Gγ are in *light gray* and *dark gray*. *B*, amino acid sequence alignment between G_{olf} and G_s short. Identical and homologous residues are highlighted in *yellow* and *green*, respectively. Insertion positions for G_s as well as G_{olf} are enclosed by *rectangles*, and the residue numbers for G_s are shown above.

G_{olf} movement extrapolated from novel G_{olf} biosensors corresponds to that of G_s

As mentioned above, the G_{olf} subunit is widely expressed in the striatum, where it is critical to the function of D1R. Taking advantage of its 89% sequence identity to G_s, luciferase or mVenus was inserted at the same nine positions explored above (Fig. 1*B*). Given their enriched expression in striatum (12, 14–17), β2 and γ7 constructs were used to study G_{olf} activation. Similar to the G_s results, both G_{olf}-Rluc-γ7-GFP10 and G_{olf}-Venus-γ7-Rluc configurations revealed an increase in BRET values at the hinge region (position 69) and a decrease in BRET values or a lack of response in the α-helical domain (positions 100 and 155) for β2AR receptor activation (Fig. 3*A* and supplemental Table S2). The same directionalities were observed for D1R, further supporting the conservation of domain movements of these homologous G proteins when activated by different receptors (Fig. 3*A* and supplemental Table S2). The results are also consistent with a large displacement of the α-helical domain in G_{olf}, similar to that observed in G_s (Fig. 2, *C* and *D*) and to the crystal structure of the active complex (2).

Development of a D1R-G_{olf} assay

To establish a reliable assay for drug screening at the D1R with regard to G_{olf} coupling, different configurations of BRET

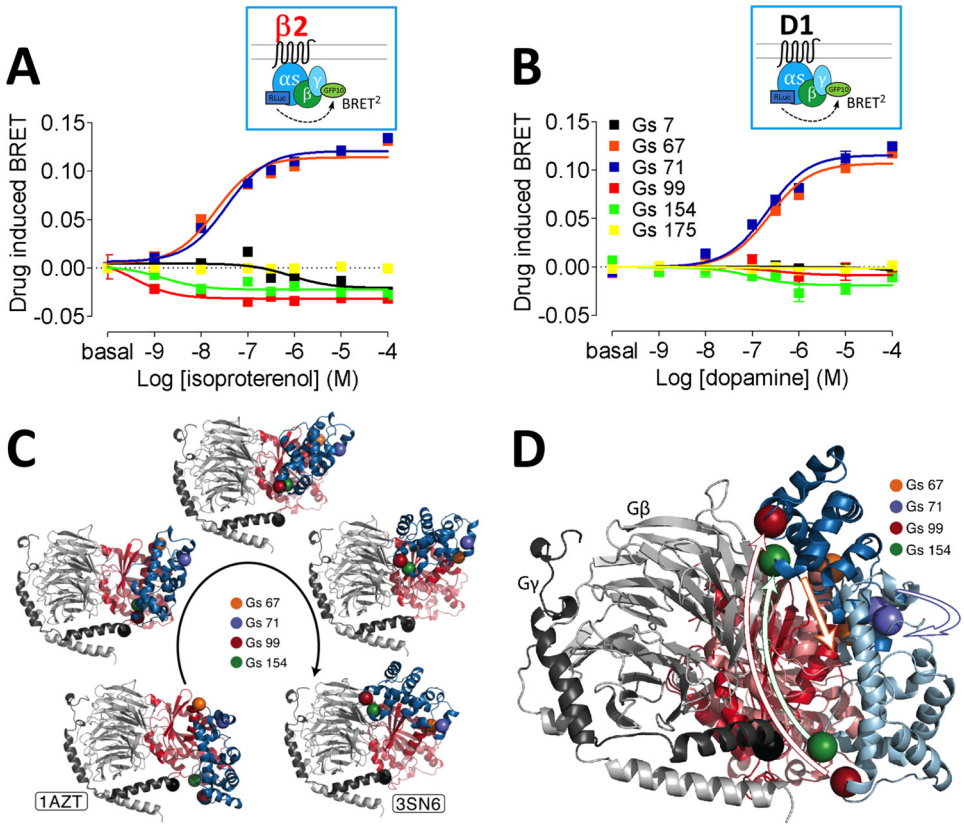

Figure 2. *A* and *B*, dose-response curves of G_s protein activation BRET for β2AR with isoproterenol (*A*) and for D1R with dopamine (*B*). Different colors represent insertion positions for Rluc: *black*, 7–8 amino acids; *orange*, 67–68 amino acids; *blue*, 71–72 amino acids; *red*, 99–100 amino acids; *green*, 154–155 amino acids; *yellow*, 175–176 amino acids. The dose-response curves represent the means ± S.E. of more than five experiments performed in triplicate. *C*, composite pictures (five frames) of the simulated transition from an inactive/closed (modeled by the 1AZT crystal structure) to an active/open (modeled by the 3SN6 crystal structure) state of the G_s subunit. Computer simulations predict transitional movement (frames 2–4) between the α-helical domain containing 99 and 154 amino acids and hinge domain (with 67 and 71 amino acids) linking the α-helical and Ras-like domains. The α-helical and Ras-like domains of Gα are in *blue* and *red*, respectively, whereas Gβ and Gγ are in *light gray* and *dark gray*. *D*, superposition of the closed and open crystal structures of the G_s protein, highlighting the movement of the G_s α-helical domain (*light* and *dark blue*, respectively, in the inactive and active conformations), with respect to the Ras-like domain (in *light* and *dark red*, respectively, in the two conformations), hinged on the region of probes 67 and 71. The *black sphere* indicates where the acceptor GFP10 is fused at the N terminus of Gγ subunit. The location of four selected probes introduced at residues 67 (*orange*), 71 (*blue*), 99 (*red*), and 154 (*green*) are indicated with *spheres*.

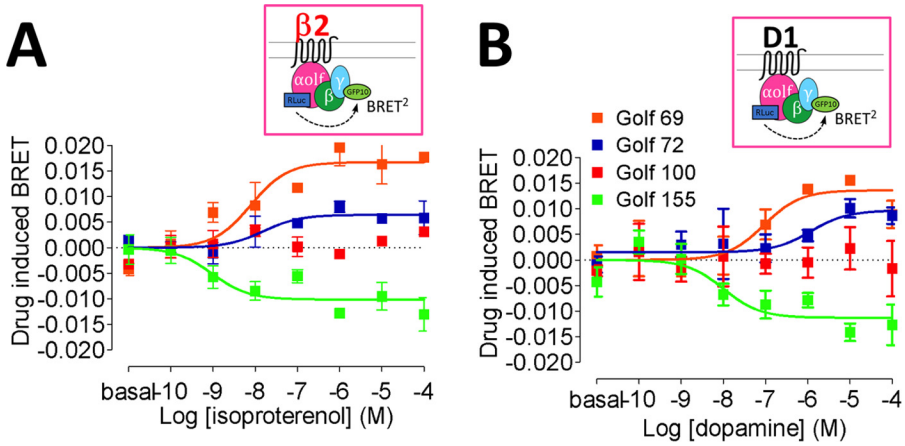

Figure 3. *A* and *B*, dose-response curves of G_{olf} protein activation BRET for β2AR with isoproterenol (*A*) and for D1R with dopamine (*B*). Different colors represent insertion positions for Rluc: *orange*, 69–70 amino acids; *blue*, 72–73 amino acids; *red*, 100–101 amino acids; *green*, 155–156 amino acids. The dose-response curves represent the means ± S.E. of more than five experiments performed in triplicate. EC_{50} values between β2AR and D1R for each of 69, 72, and 155 positions of G_{olf} sensors were compared using one-way analysis of variance with post hoc Tukey test analysis and did not reach statistical significance.

were tested (supplemental Table S2 and Fig. 4). Fig. 4 shows direct comparisons between G_s and G_{olf} biosensors in the activation and engagement modes. For Gα-γ activation assays, the relative potency and efficacy differences between dopamine, a full agonist, and norepinephrine, a less potent agonist, were tested. The potency differences between the two agonists were similar for activation of G_s and G_{olf} (Fig. 4, *A* and *B*, and supplemental Table S3). The engagement assays also demon-

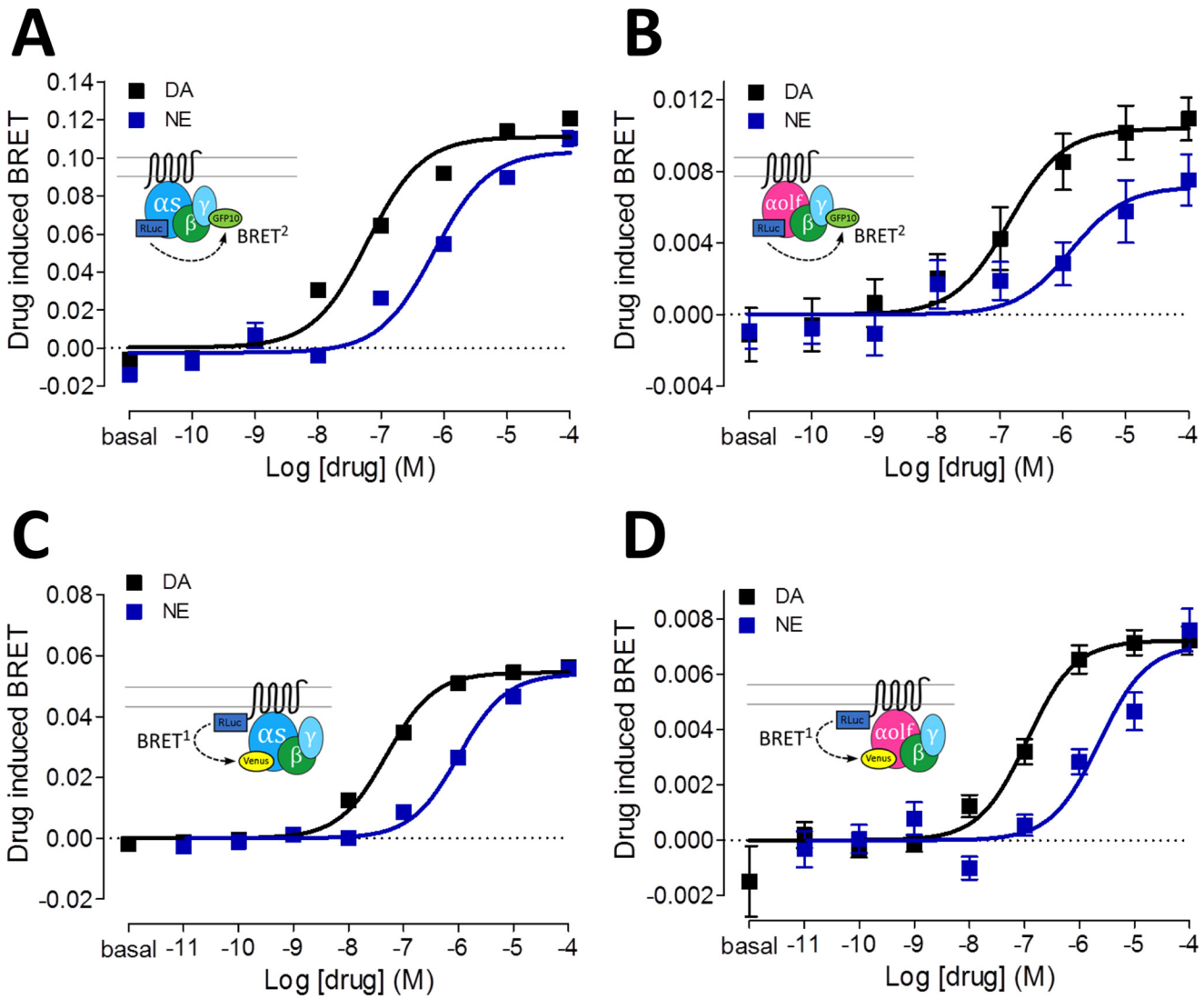

Figure 4. *A* and *B*, dose-response curves of G_s (*A*) or G_{olf} (*B*) protein activation BRET for D1R with dopamine (*black curve*) or norepinephrine (*blue curve*). *C* and *D*, dose-response curves of dopamine (*black curve*) or norepinephrine (*blue curve*) induced BRET between D1R-Rluc and G_s-Venus (*C*) or G_{olf}-Venus (*D*). Corresponding schemes are illustrated in *insets*. The dose-response curves represent the means ± S.E. of more than five experiments performed in triplicate. *DA*, dopamine; *NE*, norepinephrine.

strated a tight agreement of relative potency and efficacy between dopamine and norepinephrine in G_s and G_{olf} (Fig. 4, *C* and *D*, and supplemental Table S3).

The engagement (*i.e.* D1R-Rluc-G_{olf}-Venus) BRET configuration was pursued for optimization because of its larger dynamic window. Different β-γ subunit combinations were tested (supplemental Fig. S5). Although the β1-γ7 and β2-γ7 combinations showed a similar dynamic range, β2-γ7 was chosen for the rest of the studies because of the established expression overlap in striatum (10–13). One of the crucial factors for successful G_{olf} BRET assay regardless of configuration was co-expression of the G-protein chaperone Ric8 (18–20), which robustly enhanced the dynamic range of agonist-induced BRET (supplemental Fig. S4). Because luciferase expression, detected by luminescence, does not differ significantly with and without Ric8 co-expression, the dramatic change in dynamic range of BRET may have to do with chaperone activities of Ric8, possibly rescuing misfolding or aiding proper localization of the G_{olf} biosensor to the receptor complex rather than simply enhancing its expression (supplemental Fig. S4). Overall, cross-comparison of the D1R-Gα engagement and Gα-γ activation assays validates the potency and efficacy range of the four assays tested and thus their utility in pharmacological characterization of D1R activation.

Creation of novel homology-based G_{i1} and G_q biosensors

Because the Ras-like domain, hinge region, and α-helical domain are well-conserved in other classes of Gα subunits (21), the relative movements upon activation were compared in other Gα subunits. The same three sensor insertions (*i.e.* G_s equivalent of positions 67, 99, and 154) were made in G_{i1} and G_q at the aligned amino acid residues (Fig. 5*A*). Upon transfection with dopamine D_2 receptor (D2R) and using dopamine as ligand, for G_{i1}, the hinge region (position 60) moves closer to the γ subunit, whereas the α-helical domain (positions 91 and 145) moves away from the γ subunit (Fig. 5*B*), similar to our results in G_s (Fig. 2). The conformational changes in the hinge and α-helical domains of G_{i1} are consistent with previous

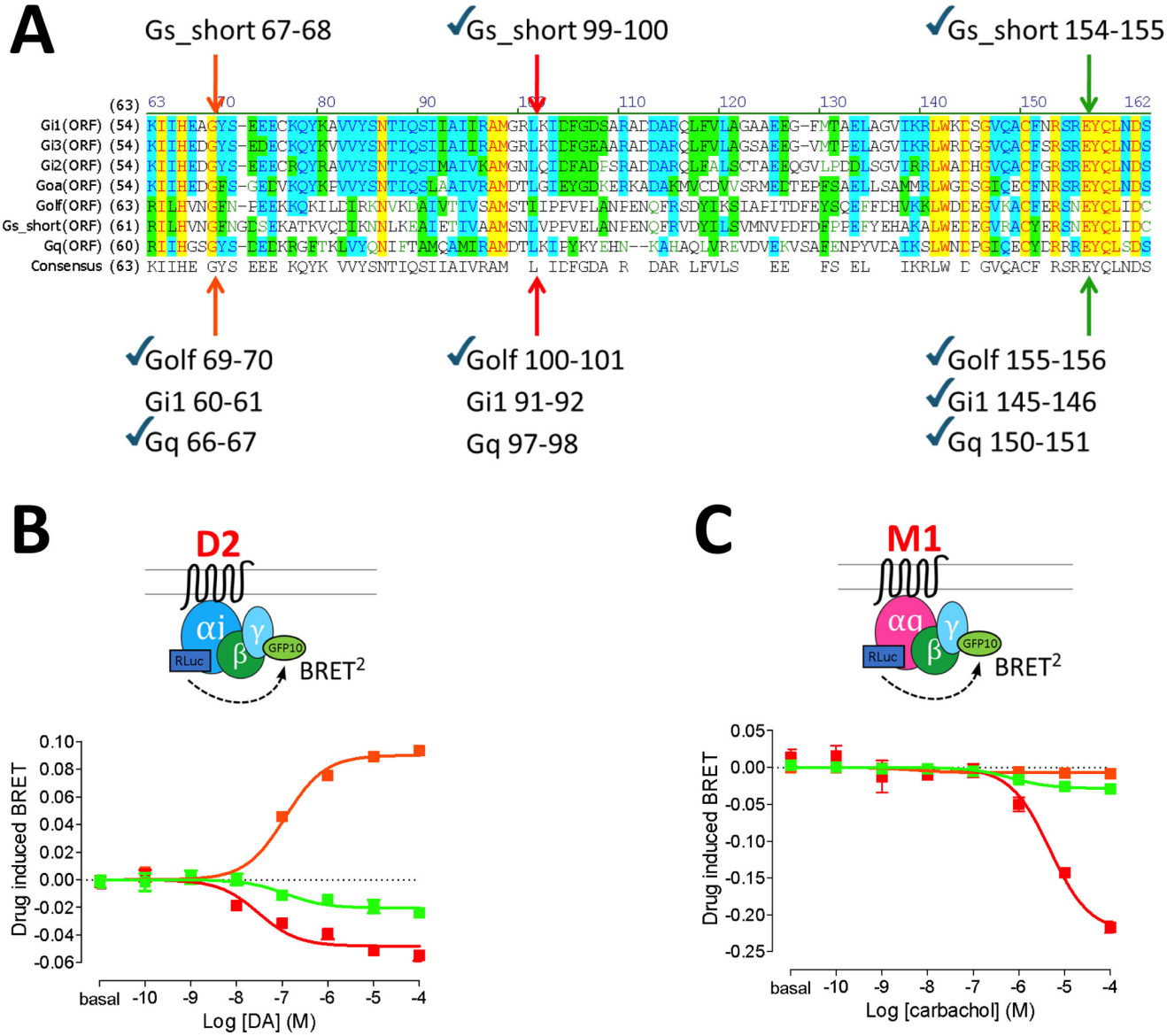

Figure 5. *A*, amino acid sequence alignment among G_{i1}, Gi2, Gi3, GoA, G_{olf}, G_s short, and G_q. Identical, highly homologous, and homologous residues are highlighted in *yellow*, *blue*, and *green*, respectively. Insertion positions equivalent to G_s short positions 67, 99, and 154 are indicated by *arrows*. Novel constructs made for this study are indicated by *check marks*. *B* and *C*, dose-response curves of G_{i1} protein activation BRET for D2R with dopamine (*B*) and G_q protein activation for muscarinic M1R with carbachol (*C*). Different colors represent insertion positions for Rluc: *orange*, 60–61 [G_{i1}] or 66–67 [G_q] amino acids; *red*, 91–92 [G_{i1}] or 97–98 [G_q] amino acids; *green*, 145–146 [G_{i1}] or 150–151 [G_q] amino acids. The dose-response curves represent the means ± S.E. of more than five experiments performed in triplicate.

reports with insertions at positions 60 and 91 (8, 9). Upon transfection with muscarinic M_1 receptor (M1R) and using carbachol as ligand, G_q sensors also revealed the same directionalities of BRET change for the α-helical domain (positions 97 and 150) (Fig. 5*C*) but with a very robust dynamic range for drug response with the position 97 sensor. However, the insertion at position 66 (equivalent to 67 in G_s) yielded very little agonist-induced BRET (Fig. 5*C*, *orange curve*), although the luminescence was similar (data not shown), suggesting a possible structural difference in the hinge loop of G_q.

Finally, using the Venus-fused G_{i1} or G_q sensors, receptor–Gα engagement BRET was assessed for D2R or M1R (supplemental Fig. S6). Consistent with the G_s results, insertion at position 150 of G_q (aligned to 154 in G_s) gave the largest efficacy window, as well as higher potency when compared with the previously characterized position 97 (22) (supplemental Fig. S6*B*). This trend was not maintained with G_{i1}, where insertion at position 91 (aligned with position 99 in G_s) produced the most robust sensor (supplemental Fig. S6*A*). Taken together, these results with G-protein activation BRET have established generally conserved movements of the α-helical domain in three different classes of Gα subunits, albeit with subtle differences.

Discussion

The seminal work leading to the crystal structure of the active β2AR-G_s heterotrimer complex has enabled comparison between open and closed structures of the G protein, as well as interactions of the G protein with the receptor, providing molecular details of key conformational changes associated

with the activation process (2, 6, 23). A series of relevant structure–function studies have pointed to the large displacement of the α-helical domain as a central mechanism, albeit not sufficient, for the promotion of GDP–GTP exchange (3–5). Although the α-helical domain may undergo spontaneous fluctuation between the open and closed states, insertion of the α5 helix of G_s into the intracellular vestibule of the β2AR promotes opening of the α-helical domain. The pronounced decrease in BRET values in living cells indicates a distancing event between the α-helical domain and the γ subunit, consistent with an opening movement from three different amino acid positions of the α-helical domain (positions 99, 154, and 175). The movement in the loop structures, which serve as a hinge between the α-helical and Ras-like domains, is therefore an important feature that links the displacement of the α-helical domain with G_s activation. Presumably because of the highly flexible nature of the linker loop, this region was not resolved in the crystal structure (2, 6). Based on our MD simulations, we hypothesize that the transition between the closed and open states of the G-protein subunit may involve an outward protruding movement of the linker loop (positions 67, 71), along with the overall structural changes that enable α-helical domain opening. The negative BRET change between the myristoylated αN loop (position 7) and γ subunit is also consistent with the displacement of αN between the opened and closed G_s crystal structures.

Similarly, α-helical domain displacement has been proposed for the G_i and G_q proteins as an activation mechanism (21). In addition to previously studied positions (G_{s71}, G_{i160}, G_{i191}, and G_{q97}) (7–9, 22, 24), we have created novel fusion constructs at G_s positions 67, 99, and 154 and equivalent positions in G_i and G_q. Because of the conserved structural domains (*i.e.* α-helical, linker loop, Ras-like domains), not surprisingly, our results mostly coincide with previous studies. In the activation configuration, only G_{q66} failed to display positive BRET changes compared with G_{i160} or G_{s67}, possibly because of a difference in the linker-loop structure that does not generate a protruding movement in G_q. Overall, the Gα-γ BRET assay demonstrates the conserved nature of α-helical domain movement across three different Gα protein subtypes and strengthens the case for these assays as robust sensors of agonist-induced activation in living cells.

In line with its specific brain distribution, G_{olf} is involved in olfaction and basal ganglia function (12, 25, 41). Mutations in the *GNAL* gene encoding Gαolf have been implicated in movement disorders in humans (26–29). Because of their high homology, G_{olf} is generally considered to function similarly to G_s in terms of its ability to stimulate adenylate cyclase. Although some kinetic difference in GTP hydrolysis has been suggested between G_s and G_{olf} in β2AR (30), to our knowledge, there has not been a thorough molecular study of its activation. The current study is the first to focus on direct comparison of D1R-G_s and D1R-G_{olf} coupling and activation. Our new findings indicate that: 1) conformational changes upon activation are similar for G_s and G_{olf}; 2) Ric8B is required for heterologous expression of G_{olf} biosensors, as reported previously (18–20); and 3) the β2–γ7 pair confers the largest dynamic range for G_{olf} engagement BRET in agreement with previous studies showing a dependence on co-expression of G_{olf}, β2, and γ7 subunits for striatal D1R and A2AR signaling (10, 13). The directionalities of the G_{olf} activation BRET at different insertion positions are for the most part consistent with the G_s results, but overall the dynamic range of agonist response is not as robust as for G_s. It is worth considering that there may be subtle differences between β2AR and D1R in G_{olf} activation because their EC_{50} values for the 69, 72, and 155 position sensors show a trend of difference, although these did not reach statistical significance.

Notably, although the Rluc or Venus expression level (measured by luminescence or fluorescence) is similar between the G_s and G_{olf} biosensors, the efficiency of folding or localization of the G_{olf} sensors may be impaired because the basal BRET is lower for D1R-Rluc-G_{olf}-Venus than for D1R-Rluc-G_s-Venus. This may explain the lack of agonist response for the position 100 insertion in G_{olf}-Rluc. The expression of G_{olf} and G_{olf} fusion constructs is likely challenging because the accessory molecules that are present in neurons may be missing in heterologous cells. Studies have indicated that co-expression of Ric8B and HSP70, both chaperone proteins, enhance the expression of both olfactory receptor and its G_{olf} signaling (31). In our hands, Ric8B increased the BRET dynamic range of BRET of G_{olf} constructs, although HSP70 did not. Perhaps expression of other accessory proteins might help to increase further the dynamic range of the G_{olf} assays.

In summary, our novel G_{olf} assay represents a useful screening method for G_{olf} signaling in heterologous cells. The G_s and G_{olf} assays presented herein can be used in parallel for pharmacological investigation of receptors relevant in neuropsychiatric disorders, including both D1R and A2AR.

Experimental procedures

DNA constructs and transfection

For all the receptor constructs, a signal peptide followed by a FLAG epitope tag was fused to the N terminus for enhanced cell surface expression (32) and detection (33). The human receptor constructs used were A2AR, D1R, β2AR, β1AR, dopamine D2 short receptor, and M1R (34). For the D1R, D2R, and M1R fusion constructs, the cDNA encoding full-length Rluc8 (provided by Dr. S. Gambhir, Stanford University, Stanford, CA) was fused in-frame to the C terminus of the receptors as reported (35). The following human G-protein constructs were used: Gαs-mVenus, Gαolf-mVenus, Gαs-Rluc, Gαolf-Rluc, $G\alpha_{i1}$-Rluc, and Gαq-Rluc whose various insertion positions were specified below. For $G\alpha_{i1}$-Rluc, Rluc was inserted at position 60, 91, or 145. For Gαq-Rluc, Rluc was inserted at position 66, 97, or 150. For Gαs-mVenus, Gαolf-mVenus, Gαs-Rluc, and Gαolf-Rluc constructs, mVenus or Rluc was inserted at positions 7 (8), 67 (69), 71 (72), 99 (100), 131 (132), 154 (155), 175 (176), 305 (306), 338 (339), 349 (350) (G_{olf} numbering in parentheses). For Gγ2 and Gγ7 fusion constructs, full-length mVenus, GFP10, or Rluc was fused at its N terminus. Untagged βγ subunits Gβ1, Gβ2, Gβ4, Gβ5, Gγ2, and Gγ7 were also used for co-transfection. The G-protein chaperone Ric8B was co-transfected with Gαs and Gαolf constructs. Ric8A was co-transfected with Gαq constructs. Ric8 plasmids were kind gifts from Dr. Gregory Tall (20, 36). All the constructs were confirmed by sequence analysis. A constant amount of total

plasmid cDNA (15 μg) was transfected into human embryonic kidney cells 293T (HEK-293T) using polyethylenimine (Sigma–Aldrich) in a 1:2 ratio in 10-cm plates. The cells were maintained in culture with Dulbecco's modified Eagle's medium supplemented with 10% fetal bovine serum and kept in an incubator at 37 °C and 5% CO_2. The transfected amount and ratio among the receptor and heterotrimeric G proteins were tested for optimized dynamic range in agonist-induced BRET. For instance, in activation and engagement BRET described below, the ratios of 3:3:4:5:2.5 (receptor:Gα-Rluc:Gβ:Gγ-GFP10:Ric8B) and 0.25:5:4:4:2.5 (receptor-Rluc:Gα-Venus:Gβ:Gγ:Ric8B) were used respectively. Experiments were performed ~48 h post-transfection.

BRET assay

Three modes of BRET assays were performed to detect receptor ligand-induced events for 1) Gα-γ protein activation, 2) Gγ–α protein activation, and 3) receptor-Gα engagement. 1) The Gα-γ protein activation assay uses a RLuc-fused Gα-protein subunit and GFP10-fused Gγ protein for a resonance energy transfer (RET) pair. FLAG-tagged receptor and untagged Gβ constructs were co-transfected. 2) Similarly the Gγ–α protein activation assay uses a RLuc-fused Gγ protein subunit and GFP10-fused Gα protein for a RET pair. FLAG-tagged receptor and untagged Gβ constructs were co-transfected. 3) The receptor-Gα engagement assay uses RLuc-fused receptor and mVenus-fused Gα protein for the RET pair. Untagged Gβ and Gγ constructs were co-transfected. As reported previously (35), cells were harvested, washed, and resuspended in PBS. Approximately 200,000 cells/well were distributed in 96-well plates, and 5 μM coelenterazine H (substrate for BRET1) or 5 μM coelenterazine 400a (substrate for BRET2) was added to each well. Three minutes after addition of coelenterazine, ligands (dopamine (Sigma), L-(−)-norepinephrine (Sigma), 5′-*N*-ethylcarboxamidoadenosine (Tocris), isoproterenol (Tocris), or carbachol (Tocris)) were added to each well. The fluorescence of the acceptor was quantified (for Venus excitation at 500 nm and emission at 530 nm for 1-s recording or for GFP10 excitation at 405 nm and emission at 515 nm for 1-s recording for GFP10) in a Mithras LB940 (Berthold Technologies, Bad Wildbad, Germany) to confirm constant expression levels across experiments. In parallel, luminescence and BRET1 signal from the same batch of cells was determined as the ratio of the light emitted by Venus (530 nm) over that emitted by coelenterazine H (485 nm) or luminescence and BRET2 signal from the same batch of cells was determined as the ratio of the light emitted by GFP10 (515 nm) over that emitted by coelenterazine 400a (400 nm). The results are calculated for the BRET change (BRET ratio for the corresponding ligand minus BRET ratio in the absence of the ligand). E_{max} values are expressed as the basal subtracted BRET change in the dose-response graphs. The fluorescence and luminescence counts (arbitrary units) were similar in different experiments using the same construct. The data and statistical analyses were performed with Prism 5 (GraphPad software).

Sequence homology alignment

Amino acid sequence homology analysis was performed using Vector NTI Advance (Invitrogen). Identical residues are highlighted *yellow*, and homologous residues are highlighted *green*.

Molecular modeling and computer simulations

The closed (PDB code 1AZT), and open (PDB code 3SN6, chains A, B, and G) crystal structures of G_s were used for MD simulations. Missing loop residues (at positions 66–72) of the closed G_s crystal structure were built using the Rosetta loop prediction algorithm (37). The best scoring conformation was extracted and equilibrated in TIP3P waters by a 20-ns MD simulation using all-atom description and the Charmm27 force field (38). The open and closed structures were used as templates to model G_{olf} by homology (39). To investigate the changes in conformation between the inactive and active conformations, an adiabatic biased MD simulation (40) was performed starting from the protein inactive state, using the RMSD from the active state model as a collective variable. Briefly, a steep repulsive bias was applied when the RMSD from the target state increased above the minimum value reached during the simulation. Specifically, the applied potential was

$$V(R(t)) = \frac{K}{2}(CV(R(t)) - CV_{\text{Min}}(R(t)))^2 \qquad \text{(Eq. 1)}$$

where the collective variable is the RMSD to the active state, and

$$CV_{\text{Min}}(R(t)) = \min_{0<s<t} CV(R(s)) + \eta(t) \qquad \text{(Eq. 2)}$$

Similar to a ratchet and pawl system, propelled by thermal motion, the biasing potential does not exert work on the system and ensures that the obtained trajectory is a low-free energy path connecting the initial and final states. The simulation was stopped after 20 ns. Simulations were performed with Gromacs 4.6 with Plumed 2.0. The simulation was carried out in the NPT ensemble, using v-rescale thermostat and Parrinello–Rahman barostat to maintain temperature and pressure constant. Electrostatics was calculated with the particle-mesh Ewald algorithm, and non-bonded interactions were cut-off at 1.2 nm. A time step of 2 fs was used. Distances between the C atoms of insertion points of the experimental probes were monitored during simulation.

Author contributions—H. Y. designed, conducted, and analyzed the molecular biology and BRET experiments. D. P. and M. F. conducted and analyzed the molecular dynamics simulation. N. S. C. performed the molecular biology work. H. Y. and J. A. J. wrote the manuscript. All authors contributed to reviewing the results and writing the manuscript.

Acknowledgments—We thank Gregory Tall for the Ric8 constructs; Nevin Lambert for the G_{i1}_91_mVenus and G_q_97_mVenus constructs and helpful comments on cloning; and Céline Gales for G_{i1}_60_Rluc8, G_{i1}_91_Rluc8, and G_q_97_Rluc8 constructs. Computer simulations were run on resources available through the Scientific Computing Facility at Mount Sinai and the Extreme Science and Engineering Discovery Environment under Program MCB080077, which is supported by National Science Foundation Grant ACI-1053575.

References

1. Lein, E. S., Hawrylycz, M. J., Ao, N., Ayres, M., Bensinger, A., Bernard, A., Boe, A. F., Boguski, M. S., Brockway, K. S., Byrnes, E. J., Chen, L., Chen, L., Chen, T.-M., Chin, M. C., Chong, J., *et al.* (2007) Genome-wide atlas of gene expression in the adult mouse brain. *Nature* **445,** 168–176
2. Rasmussen, S. G., DeVree, B. T., Zou, Y., Kruse, A. C., Chung, K. Y., Kobilka, T. S., Thian, F. S., Chae, P. S., Pardon, E., Calinski, D., Mathiesen, J. M., Shah, S. T., Lyons, J. A., Caffrey, M., Gellman, S. H., *et al.* (2011) Crystal structure of the β_2 adrenergic receptor-G_s protein complex. *Nature* **477,** 549–555
3. Chung, K. Y., Rasmussen, S. G., Liu, T., Li, S., DeVree, B. T., Chae, P. S., Calinski, D., Kobilka, B. K., Woods, V. L., Jr., and Sunahara, R. K. (2011) Conformational changes in the G protein G_s induced by the β_2 adrenergic receptor. *Nature* **477,** 611–615
4. Westfield, G. H., Rasmussen, S. G., Su, M., Dutta, S., DeVree, B. T., Chung, K. Y., Calinski, D., Velez-Ruiz, G., Oleskie, A. N., Pardon, E., Chae, P. S., Liu, T., Li, S., Woods, V. L., Jr., Steyaert, J., *et al.* (2011) Structural flexibility of the $G\alpha_s$ α-helical domain in the β_2-adrenoceptor G_s complex. *Proc. Natl. Acad. Sci. U.S.A.* **108,** 16086–16091
5. Dror, R. O., Mildorf, T. J., Hilger, D., Manglik, A., Borhani, D. W., Arlow, D. H., Philippsen, A., Villanueva, N., Yang, Z., Lerch, M. T., Hubbell, W. L., Kobilka, B. K., Sunahara, R. K., and Shaw, D. E. (2015) Structural basis for nucleotide exchange in heterotrimeric G proteins. *Science* **348,** 1361–1365
6. Sunahara, R. K., Tesmer, J. J., Gilman, A. G., and Sprang, S. R. (1997) Crystal structure of the adenylyl cyclase activator $G_s\alpha$. *Science* **278,** 1943–1947
7. Yu, J.-Z., and Rasenick, M. M. (2002) Real-time visualization of a fluorescent G_s: dissociation of the activated G protein from plasma membrane. *Mol. Pharmacol.* **61,** 352–359
8. Galés, C., Rebois, R. V., Hogue, M., Trieu, P., Breit, A., Hébert, T. E., and Bouvier, M. (2005) Real-time monitoring of receptor and G-protein interactions in living cells. *Nat. Methods* **2,** 177–184
9. Galés, C., Van Durm, J. J., Schaak, S., Pontier, S., Percherancier, Y., Audet, M., Paris, H., and Bouvier, M. (2006) Probing the activation-promoted structural rearrangements in preassembled receptor-G protein complexes. *Nat. Struct. Mol. Biol.* **13,** 778–786
10. Schwindinger, W. F., Betz, K. S., Giger, K. E., Sabol, A., Bronson, S. K., and Robishaw, J. D. (2003) Loss of G protein γ7 alters behavior and reduces striatal G_{olf} level and cAMP production. *J. Biol. Chem.* **278,** 6575–6579
11. Xie, K., Masuho, I., Shih, C.-C., Cao, Y., Sasaki, K., Lai, C. W., Han, P.-L., Ueda, H., Dessauer, C. W., Ehrlich, M. E., Xu, B., Willardson, B. M., and Martemyanov, K. A. (2015) Stable G protein-effector complexes in striatal neurons: mechanism of assembly and role in neurotransmitter signaling. *eLife* **4,** e10451
12. Hervé, D. (2011) Identification of a specific assembly of the G protein G_{olf} as a critical and regulated module of dopamine and adenosine-activated cAMP pathways in the striatum. *Front. Neuroanat.* **5,** 48
13. Schwindinger, W. F., Mihalcik, L. J., Giger, K. E., Betz, K. S., Stauffer, A. M., Linden, J., Herve, D., and Robishaw, J. D. (2010) Adenosine A2A receptor signaling and G_{olf} assembly show a specific requirement for the γ7 subtype in the striatum. *J. Biol. Chem.* **285,** 29787–29796
14. Corvol, J. C., Studler, J. M., Schonn, J. S., Girault, J. A., and Hervé, D. (2001) $G\alpha_{olf}$ is necessary for coupling D1 and A2a receptors to adenylyl cyclase in the striatum. *J. Neurochem.* **76,** 1585–1588
15. Hervé, D., Le Moine, C., Corvol, J.-C., Belluscio, L., Ledent, C., Fienberg, A. A., Jaber, M., Studler, J.-M., and Girault, J.-A. (2001) $G\alpha_{olf}$ levels are regulated by receptor usage and control dopamine and adenosine action in the striatum. *J. Neurosci.* **21,** 4390–4399
16. Hervé, D., Lévi-Strauss, M., Marey-Semper, I., Verney, C., Tassin, J. P., Glowinski, J., and Girault, J. A. (1993) G_{olf} and G_s in rat basal ganglia: possible involvement of G_{olf} in the coupling of dopamine D1 receptor with adenylyl cyclase. *J. Neurosci.* **13,** 2237–2248
17. Zhuang, X., Belluscio, L., and Hen, R. (2000) $G_{olf}\alpha$ mediates dopamine D1 receptor signaling. *J. Neurosci.* **20,** RC91
18. Chan, P., Gabay, M., Wright, F. A., Kan, W., Oner, S. S., Lanier, S. M., Smrcka, A. V., Blumer, J. B., and Tall, G. G. (2011) Purification of heterotrimeric G protein α subunits by GST-Ric-8 association: primary characterization of purified $G\alpha_{olf}$. *J. Biol. Chem.* **286,** 2625–2635
19. Gabay, M., Pinter, M. E., Wright, F. A., Chan, P., Murphy, A. J., Valenzuela, D. M., Yancopoulos, G. D., and Tall, G. G. (2011) Ric-8 proteins are molecular chaperones that direct nascent G protein α subunit membrane association. *Sci. Signal.* **4,** ra79
20. Von Dannecker, L. E., Mercadante, A. F., and Malnic, B. (2005) Ric-8B, an olfactory putative GTP exchange factor, amplifies signal transduction through the olfactory-specific G-protein $G\alpha_{olf}$. *J. Neurosci.* **25,** 3793–3800
21. Oldham, W. M., and Hamm, H. E. (2008) Heterotrimeric G protein activation by G-protein–coupled receptors. *Nat. Rev. Mol. Cell Biol.* **9,** 60–71
22. Qin, K., Dong, C., Wu, G., and Lambert, N. A. (2011) Inactive-state preassembly of G_q-coupled receptors and G_q heterotrimers. *Nat. Chem. Biol.* **7,** 740–747
23. Rosenbaum, D. M., Cherezov, V., Hanson, M. A., Rasmussen, S. G., Thian, F. S., Kobilka, T. S., Choi, H. J., Yao, X. J., Weis, W. I., Stevens, R. C., and Kobilka, B. K. (2007) GPCR engineering yields high-resolution structural insights into β_2 adrenergic receptor function. *Science* **318,** 1266–1273
24. Hughes, T. E., Zhang, H., Logothetis, D. E., and Berlot, C. H. (2001) Visualization of a functional $G\alpha_q$-green fluorescent protein fusion in living cells: association with the plasma membrane is disrupted by mutational activation and by elimination of palmitoylation sites, but not by activation mediated by receptors or AlF_4. *J. Biol. Chem.* **276,** 4227–4235
25. Jones, D. T., and Reed, R. R. (1989) G_{olf}: an olfactory neuron specific-G protein involved in odorant signal transduction. *Science* **244,** 790–795
26. Kumar, K. R., Lohmann, K., Masuho, I., Miyamoto, R., Ferbert, A., Lohnau, T., Kasten, M., Hagenah, J., Brüggemann, N., Graf, J., Münchau, A., Kostic, V. S., Sue, C. M., Domingo, A. R., Rosales, R. L., *et al.* (2014) Mutations in gnal: a novel cause of craniocervical dystonia. *JAMA Neurol.* **71,** 490–494
27. Corradi, J. P., Ravyn, V., Robbins, A. K., Hagan, K. W., Peters, M. F., Bostwick, R., Buono, R. J., Berrettini, W. H., and Furlong, S. T. (2005) Alternative transcripts and evidence of imprinting of GNAL on 18p11.2. *Mol. Psychiatry* **10,** 1017–1025
28. Fuchs, T., Saunders-Pullman, R., Masuho, I., Luciano, M. S., Raymond, D., Factor, S., Lang, A. E., Liang, T.-W., Trosch, R. M., White, S., Ainehsazan, E., Hervé, D., Sharma, N., Ehrlich, M. E., Martemyanov, K. A., *et al.* (2013) Mutations in GNAL cause primary torsion dystonia. *Nat. Genet.* **45,** 88–92
29. Vemula, S. R., Puschmann, A., Xiao, J., Zhao, Y., Rudzińska, M., Frei, K. P., Truong, D. D., Wszolek, Z. K., and LeDoux, M. S. (2013) Role of $G\alpha_{olf}$ in familial and sporadic adult-onset primary dystonia. *Hum. Mol. Genet.* **22,** 2510–2519
30. Liu, H.-Y., Wenzel-Seifert, K., and Seifert, R. (2001) The olfactory G protein $G\alpha_{olf}$ possesses a lower GDP-affinity and deactivates more rapidly than $G_s\alpha$short: consequences for receptor-coupling and adenylyl cyclase activation. *J. Neurochem.* **78,** 325–338
31. Zhuang, H., and Matsunami, H. (2007) Synergism of accessory factors in functional expression of mammalian odorant receptors. *J. Biol. Chem.* **282,** 15284–15293
32. Guan, X. M., Kobilka, T. S., and Kobilka, B. K. (1992) Enhancement of membrane insertion and function in a type IIIb membrane protein following introduction of a cleavable signal peptide. *J. Biol. Chem.* **267,** 21995–21998
33. Guo, W., Urizar, E., Kralikova, M., Mobarec, J. C., Shi, L., Filizola, M., and Javitch, J. A. (2008) Dopamine D2 receptors form higher order oligomers at physiological expression levels. *EMBO J.* **27,** 2293–2304
34. Frederick, A. L., Yano, H., Trifilieff, P., Vishwasrao, H. D., Biezonski, D., Mészáros, J., Urizar, E., Sibley, D. R., Kellendonk, C., Sonntag, K. C., Graham, D. L., Colbran, R. J., Stanwood, G. D., and Javitch, J. A. (2015) Evidence against dopamine D1/D2 receptor heteromers. *Mol. Psychiatry* **20,** 1373–1385
35. Urizar, E., Yano, H., Kolster, R., Galés, C., Lambert, N., and Javitch, J. A. (2011) CODA-RET reveals functional selectivity as a result of GPCR heteromerization. *Nat. Chem. Biol.* **7,** 624–630

36. Tall, G. G., Krumins, A. M., and Gilman, A. G. (2003) Mammalian Ric-8A (synembryn) is a heterotrimeric Gα protein guanine nucleotide exchange factor. *J. Biol. Chem.* **278,** 8356–8362
37. Mandell, D. J., Coutsias, E. A., and Kortemme, T. (2009) Sub-angstrom accuracy in protein loop reconstruction by robotics-inspired conformational sampling. *Nat. Methods* **6,** 551–552
38. Best, R. B., Zhu, X., Shim, J., Lopes, P. E., Mittal, J., Feig, M., and Mackerell, A. D., Jr. (2012) Optimization of the additive CHARMM all-atom protein force field targeting improved sampling of the backbone ϕ, ψ and side-chain $\chi1$ and $\chi2$ dihedral angles. *J. Chem. Theory Comput.* **8,** 3257–3273
39. Sali, A., and Blundell, T. L. (1993) Comparative protein modelling by satisfaction Of spatial Restraints. *J. Mol. Biol.* **234,** 779–815
40. Marchi, M., and Ballone, P. (1999) Adiabatic bias molecular dynamics: a method to navigate the conformational space of complex molecular systems. *J. Chem. Physics* **110,** 3697–3702
41. Belluscio, L., Gold, G. H., Nemes, A., and Axel, R. (1998) Mice deficient in G_{olf} are anosmic. *Neuron* **20,** 69–81